Journal of Power Sources 645 (2025) 237184



Contents lists available at ScienceDirect

Journal of Power Sources

journal homepage: www.elsevier.com/locate/jpowsour





Coupling differential voltage analysis and distribution of relaxation times I: Evaluating the impact of NMC811 coating in the degradation of NMC811/Gr cells

Matheus Leal de Souza [a,b,c,*], Mathieu Morcrette [a,b,**]

[a] Laboratoire de Réactivité et de Chimie des Solides (LRCS), UMR CNRS 7314, Université de Picardie Jules Verne, HUB de l'Énergie, 80039, Amiens, Cedex 1, France
[b] Réseau sur le Stockage Électrochimique de l'Énergie (RS2E), CNRS FR 3459, France
[c] Department of Mechanical Engineering, Imperial College London, London, SW7 2AZ, UK

HIGHLIGHTS

- DVA and DRT coupling approach tracked electrodes contribution to degradation.
- NMC particle coating prevented loss of mass and slowed down cell impedance increase.
- Non-invasive operando approach tracks the evolution of the degradation effects.

ARTICLE INFO

Keywords:
DVA
DRT
Coupling
Degradation
Electrochemistry
Li-ion batteries

ABSTRACT

This paper focuses on the coupling of the Differential Voltage Analysis (dV/dQ vs Q) and the Distribution of Relaxation Times (DRT), whose benefits to electrodes development are illustrated by the tracking of degradation effects in the cycling aging of NMC811/Gr coin cells, with and without an NMC electrode coating. The former technique allows monitoring of individual electrode loss of active material (LAM), chemistry change and state of charge (SOC) alignment of the electrodes, whose variation is related mainly to loss of Li inventory (LLI). DRT is a time domain representation of the impedance that offers a high resolution of the resistance processes, complementing the DVA analysis by bringing kinetics degradation of the cells and by identifying in which electrode the main resistance processes are originated. The protocol inserting those techniques in an aging regime is a non-invasive approach, and it indicated the consumption of Li^+ ions as the main reason for capacity decay in both cells, with reduced or minimal NMC LAM and chemistry change when coating is applied. From the perspective of power decay, the coating decelerated the impedance rise (IR), mostly related to resistance processes in the positive electrode.

1. Introduction

The Li-ion batteries (LIBs) have an established competitive position in the market of secondary batteries due to its relative high energy density and flexible use [1]. However, performance of current commercialized chemistries is insufficient for the urgent and growing demands of energy storage, notably from the mobility sector [2,3]. Electric vehicles are desired to reach longer driving range after complete charge, and to be charged faster (<10 min), both attributes that can be attained by increasing the energy and power densities of their batteries. For this purpose, one of the most applied strategies in the classic LIBs that contain liquid organic electrolytes and intercalation electrodes is the employ of active materials with superior capacity density and/or higher operational voltage [4].

LIBs energy density is mainly limited by the cathodes, primary source of Li^+ ions, and recent studies have focused on layered transition metal oxides known as NMCs ($LiNi_xMn_yCo_{1-x-y}O_2$) for high energy density applications [5]. With a potential range compatible to most of the

* Corresponding author. Department of Mechanical Engineering, Imperial College London, Exhibition Road, London SW7 2AZ, United Kingdom.
** Corresponding author. Laboratoire de Réactivité et de Chimie des Solides (LRCS), UMR CNRS 7314, Université de Picardie Jules Verne, HUB de l'Énergie, 80039, Amiens, Cedex 1, France.
E-mail addresses: m.leal-de-souza@imperial.ac.uk (M. Leal de Souza), mathieu.morcrette@u-picardie.fr (M. Morcrette).

https://doi.org/10.1016/j.jpowsour.2025.237184
Received 4 February 2025; Received in revised form 11 April 2025; Accepted 23 April 2025
Available online 27 April 2025
0378-7753/© 2025 The Authors. Published by Elsevier B.V. This is an open access article under the CC BY license (http://creativecommons.org/licenses/by/4.0/).

current commercial electrolytes (reaching up to 4.3V vs Li^+/Li), a richer content in Ni for the NMC follows gains in energy density at the cost of lower thermal and chemical stabilities, turning the commercialization of the Ni-richer versions more difficult [6,7]. Electrolyte oxidation at the surface of the electrode, causing loss of lattice O_2 and forming O-poor inactive species (spinel and rock-salt), as well as particle cracking from anisotropic volume variation tend to be enhanced by higher Ni contents in NMCs [8–10]. To overcome those difficulties, the use of particle coatings proved to be an efficient strategy in improving cyclability [11–13]. Nevertheless, such a solution is viable and recommended only if the degradation mechanisms are well known, to minimize costs and eventual energy density losses due to the coating. Also, the process of optimizing coatings involves identifying and tracking its effects on the electrode during operational conditions, which can be attained by using electrochemical techniques.

A recurrent tool to evaluate the energy density of a cell is by analyzing the area of its V vs Q curve [4,14]. At a fixed temperature and quasistatic conditions, the reversible process of lithiation of an intercalation material has an open circuit potential that is dependent on the difference of chemical potentials of Li in the positive and in the negative electrodes. If the counter electrode is an ideal reference electrode, the V vs Q curve is then characteristic of the working electrode, and any degradation results in its curve modification [15]. If the counter-electrode is not an ideal reference electrode, such as with the labeled "full-cells", the V vs Q reversible curve can be determined by a fitting using the respective curves of the cell's cathodes and anodes cycled versus Li foil reference electrode under low current densities as in the approximate relation

$$V_{full-cell} = V_{+,Li} - V_{-,Li}$$

The total capacity of each electrode, related to its mass, and their effective capacity windows alignment can be tracked in order to follow loss of active material (LAM) and loss of Li inventory (LLI) if the full-cell curve is successfully reconstructed from its electrodes half-cell curves [16–18]. Therefore, the lithiation state of each electrode for a determined SOC of the full-cell is a parameter to analyze the degradation, and the variation of the electrodes lithiation states to the other for a given SOC of the cell is referred to as slippage. Inherently, one unique slippage is attributed to a cell if two degradation states or states-of-health (SOH) are compared, but for practical reasons, it can be monitored at each SOH by the non-accessed capacity of one electrode at the end of the full-cell discharge (or the offset between the full-cell 0 % SOC and their electrodes 0 % SOC), referred to as the electrode's slippage [19–21].

Differential Voltage Analysis (dV/dQ vs Q) visually magnifies any variation to the V vs Q curves and also shares a linear relation

$$\frac{dV_{full-cell}}{dQ} = \frac{dV_{+,Li}}{dQ} - \frac{dV_{-,Li}}{dQ}$$

making it easier to visualize the curves features for the fitting process. It has been largely employed by some groups for almost two decades and recently turned into a more conventional technique in degradation analysis [20–22].

DVA captures degradation from close-to-equilibrium conditions, but LIBs can be charged or partially charged at relatively high current densities, which deviates their V vs Q curves from the OCV curve due to ohmic drop and polarization arising from cell impedance [23,24]. These kinetic limitations can impose considerable penalty to energy in high power application and trigger parasitic reactions while remaining unnoticed in low current density analysis [23].

Distribution of Relaxation Times (DRT) can act complementarily to DVA by identifying which electrodes are involved in the main kinetic degradation processes, using a time-domain impedance representation independent of equivalent circuit models and with higher resolution than the conventional Nyquist or Bode plots [25–28]. The method represents the impedance function as a series of infinite RC-elements, each one with its time constant and characteristic frequency

$$\tau = RC = \frac{1}{2\pi f}$$

and related by the distribution function $\gamma(\tau)$ as

$$Z(\omega) = R_{pol}\int_{-\infty}^{\infty}\frac{\gamma(\tau)}{1+j\omega\tau}dln\tau\ ;\ \int_{-\infty}^{\infty}\tau\gamma(\tau)dln\tau = 1$$

In the equation, the term R_{pol} refers to the total polarization of the processes that can be modelled as such, so bulk resistance of the cell, pure capacitive impedance at low frequencies and pure inductive branches need to be modelled and subtracted prior to application of the conversion [26,27,29]. The integrand of the impedance expression represents the fraction of the polarization resistance whose relaxation times logarithm is within an infinitesimal interval $dln\tau$ centered in $ln\tau$, making the area of the DRT peaks a quantitative representation of the resistance associated with its process [27,29,30].

Focusing on the electrochemistry analysis of capacity and power degradation, the impact of coating a NMC811 ($LiNi_{0.8}Mn_{0.1}Co_{0.1}O_2$) electrode to NMC811/Gr cells capacity retention during cycling is studied in terms of thermodynamics and kinetics. For that, DVA and DRT are coupled to characterize variations in electrodes V vs Q curves and impedance as a function of SOC at different degrees of aging. NMC811/Li, Coated NMC811/Li and Gr/Li have their reversible V vs Q curves and DRT peaks as a function of SOC after formation cycles obtained to, respectively, reconstruct V vs Q curves and identify electrodes individual resistance contribution in NMC811/Gr and Coated NMC811/Gr cells. LLI could be identified in both cells, with clear differences in NMC811 LAM and resistance buildup in absence of the coating, proving the approach, still underexploited in battery research [31,32], is very useful for monitoring high energy density LIBs cells performance decay.

2. Experimental

2.1. Material description

The uncoated NMC811 electrode was obtained from Umicore, Belgium, and it is composed of 95 wt% NMC811 (Umicore), 3 wt% carbon black Super C65 (Imerys) and 2 wt% polyvinylidene difluoride PVDF (Sigma-Aldrich) in Al foil. It presents 32.6 % of geometric porosity, first charge of 1.17 mAh/cm^2 (245 mAh/g) and reversible discharge of 1.02 mAh/cm^2 (213 mAh/g) during formation cycles (2.5–4.3V, 25.2 °C ± 0.2 °C). Coated NMC811 electrode was manufactured in a prototyping scale roll-to-roll coating machine, using 94 wt% Coated NMC811 (Umicore), 3 wt% carbon black Super C45 (Imerys) and 3 wt% polyvinylidene difluoride PVDF (Sigma-Aldrich) in Al foil. It presents 37 % of geometric porosity, calculated from the picnometric density of the materials, first charge of 1.18 mAh/cm^2 (226 mAh/g) and reversible discharge of 1.04 mAh/cm^2 (199 mAh/g) during formation cycles. Gr electrode was obtained from Cidetec, Spain, and it is composed of 94 wt% Graphite GHDR 15-4 (Imerys), 2 wt% carbon black Super C45 (Imerys), 2 wt% carboxymethylcellulose CMC (Chempoint W2000 3 %) and 2 wt% styrene butadiene rubber SBR (Zeon BM451 B 40 %) in Cu foil. It presented 30 % porosity, first discharge of 1.26 mAh/cm^2 (401 mAh/g) and reversible charge of 1.15 mAh/cm^2 (366 mAh/g) during formation cycles (0.01–1.50V, 25.2 °C ± 0.2 °C). That way, all full-cells had approximately N/P = 1.2 as total capacity ratio between negative electrode first reduction and positive electrode first oxidation Polypropylene monolayer thin film (Celgard 2500) was employed as separator. Electrolyte consisted of 1M $LiPF_6$ in EC:EMC (30 %:70 % wt: wt) + 2 wt% VC (E-Lyte, Germany), labeled LP57 + 2 % VC. Li foil electrode is 0.38 mm thick (Sigma-Aldrich Chemistry, USA).

2.2. Coin cell assembly

2032-type cells were assembled in Ar-filled glovebox (0.1 ppm O_2,

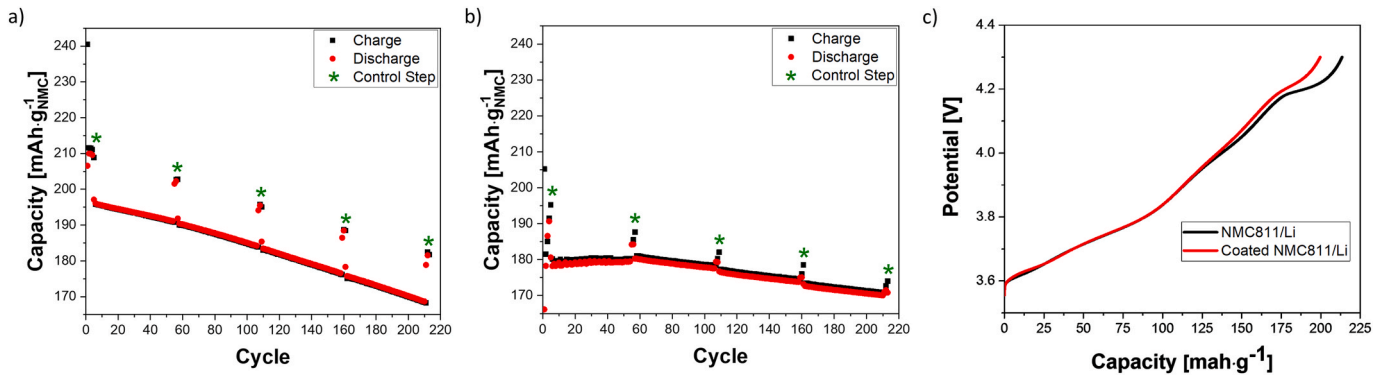


Fig. 1. Capacity vs Cycle of a) a NMC811/Gr cell a), and of b) a Coated NMC811/Gr cell, highlighting control steps in green. c) comparison of control step V vs Q curves of NMC811/Li and Coated NMC811/Li.

0.1 ppm H_2O), using one wave spring under the stainless-steel spacer of 0.5 mm thick placed under the negative electrode, and another spacer of 1.0 mm thick on the top of the positive electrode. Only one Celgard 2500 film of 16.5 mm diameter was placed between the 15 mm diameter electrodes. To improve the wetting process and minimize electrolyte flow to the empty spaces of the coin cell, half of its volume was added directly over the negative electrode, and the other half over the separator. Choice of electrolyte volume was based on 6 times the sum of porous volumes of electrodes and separator: NMC811/Li – 22.6 µl, Gr/Li – 23.6 µl, NMC811/Gr – 28.6 µl, Coated NMC811/Li – 25.2 µl, Coated NMC811/Gr – 31.2 µl, and Li symmetric cell had 20 µl, 7 times its porosity. All full-cells were loaded to have approximately 1 mAh/cm^2 of reversible capacity, with the half-cells of its respective electrodes presenting similar masses of active material: NMC811/Li – 6.35 mg, Gr/Li – 4.17 mg, NMC811/Gr – 6.73/4.26 mg, Coated NMC811/Li – 6.95 mg, and Coated NMC811/Gr – 6.67/4.08 mg. Electrodes had 13 mm diameter, except the Li, which had 14 mm diameter.

2.3. Cells aging protocol

All the cells were aged in a thermal chamber (Binder, Germany) at 25.2 °C ± 0.2 °C, and cycled in a VMP2 Potentiostat (BioLogic, France), considering 1C = 1 mA/cm^2 as current density notation, applied to all the cells. Potential windows for cycling were 2.50 V–4.20 V for the full-cells, 2.50 V–4.30 V for the positive half-cells, and 1.50 V–0.01 V for the negative half-cells. Those cutoff potentials were employed in the formation cycles and in cycling. Since the cells have relatively low loading, 6h of OCV in the chamber prior to formation cycles were considered enough for wettability. Formation cycles consisted of 3 cycles of constant current charge of C/10 and a constant voltage charge with i_{cutoff} < C/50 (CCCV charge), followed by a C/10 discharge, the last discharged following a 45 min OCV. In the sequence, full-cells underwent a first control step that alternates with 20 aging cycles of CCCV 1C, i_{cutoff} < C/20 charge and 1C discharge. The last discharge before each control step is at C/10 and followed by 45 min OCV, otherwise charge and discharge are separated by 5 min OCV. Control step has an initial C/20 charge, a C/10 discharge +45 min OCV and a PEIS step (200 kHz–10 mHz, ΔV = 7.07 mV rms, 10 points/decade, 3 measures average) that will be repeated after each pulse charge of C/20 for 2h until charge cutoff potential is reached. In the end, a 1C discharge enchains the aging cycles. Half-cell only passes formation cycles and one control step, with the Gr/Li cells protocol inverting the phase of charge for discharge. Li symmetric cell is charged and discharged for the same capacity extent of the full-cells (≅ 1.327 mAh) and using the same current density notation in 2 cycles of C/10 followed by consecutive pulse C/20 charges for 2 h followed by 30 min OCV and PEIS step in the same terms of other cells. Each cell was replicated at least twice, being one cell with representative SOH evolution at the end of the protocol undergoing further DVA and DRT analysis.

2.4. DVA fitting

The OCV V vs Q and dV/dQ vs Q curves of NMC811/Li charge and Gr/Li discharge at C/20 are obtained during the initial half of the half-cells control step. Using the Electrochemistry Visualization Application free software (EVA) [33], those curves are used to fit the experimental full-cell data and evaluate its electrodes masses and alignment (slippage) for each control step. As this fitting model is based on capturing the Li (de)insertion curves of the materials, parasitic reactions should be minimized, turning at first contradictory the choice of the charge (discharge for Gr/Li) over the discharge profile, as it is in the former that resides most of the reported degradation mechanisms [34]. However, it was taken to avoid the variation of Gr/Li delithiation V vs Q curve to the decreasing initial lithiation state, expected to occur in case of Li^+ ions consumption in the course of cycling [35]. To avoid residual kinetic interferences from the cycles with higher currents, a C/10 discharge was applied before all the control steps. As the model also considers electrodes in series, they presented the same diameter to prevent inhomogeneous reaction in the overhang [36,37].

2.5. Distribution of relaxation times

DRT is converted from the SOC dependent PEIS of all cells using the RelaxIS3 Impedance Spectrum Analysis software (RHD Instruments, Germany). Low frequency mathematical fitting and subtraction are applied to PEIS at 0 % SOC, meanwhile in other SOCs such procedures were not applied, being the DRT in the frequency of interest restricted to the range 200 kHz–0.2 Hz. Regularization parameter λ [38] was adopted as 10^{-3} for all cells and 10^{-2} for the Li symmetric cell.

3. Results and discussion

3.1. Capacity retention and V vs Q curves

In Fig. 1a, the NMC811/Gr cell presents a total (reversible + irreversible) charge capacity of 240 mAh/g in the first cycle and 210 mAh/g of discharge capacity at the end of the formation cycles. During the aging protocol, the cell presented an approximately linear capacity degradation, reaching 86 % SOH in this step after 210 cycles. Meanwhile, its coated counterpart in Fig. 1b showed 39 mAh/g of irreversible capacity in the first cycle and increasing discharge capacity during formation cycles, resulting in stable 190 mAh/g in the end of this cycling step. For the following aging protocol, a 95 % SOH was obtained after 210 cycles in this step. Fig. 1c assigns the differences in the V vs Q curves of the Coated NMC811/Li and NMC811/Li when cycled with low current density (C/20) past formation cycles. The coated positive electrode

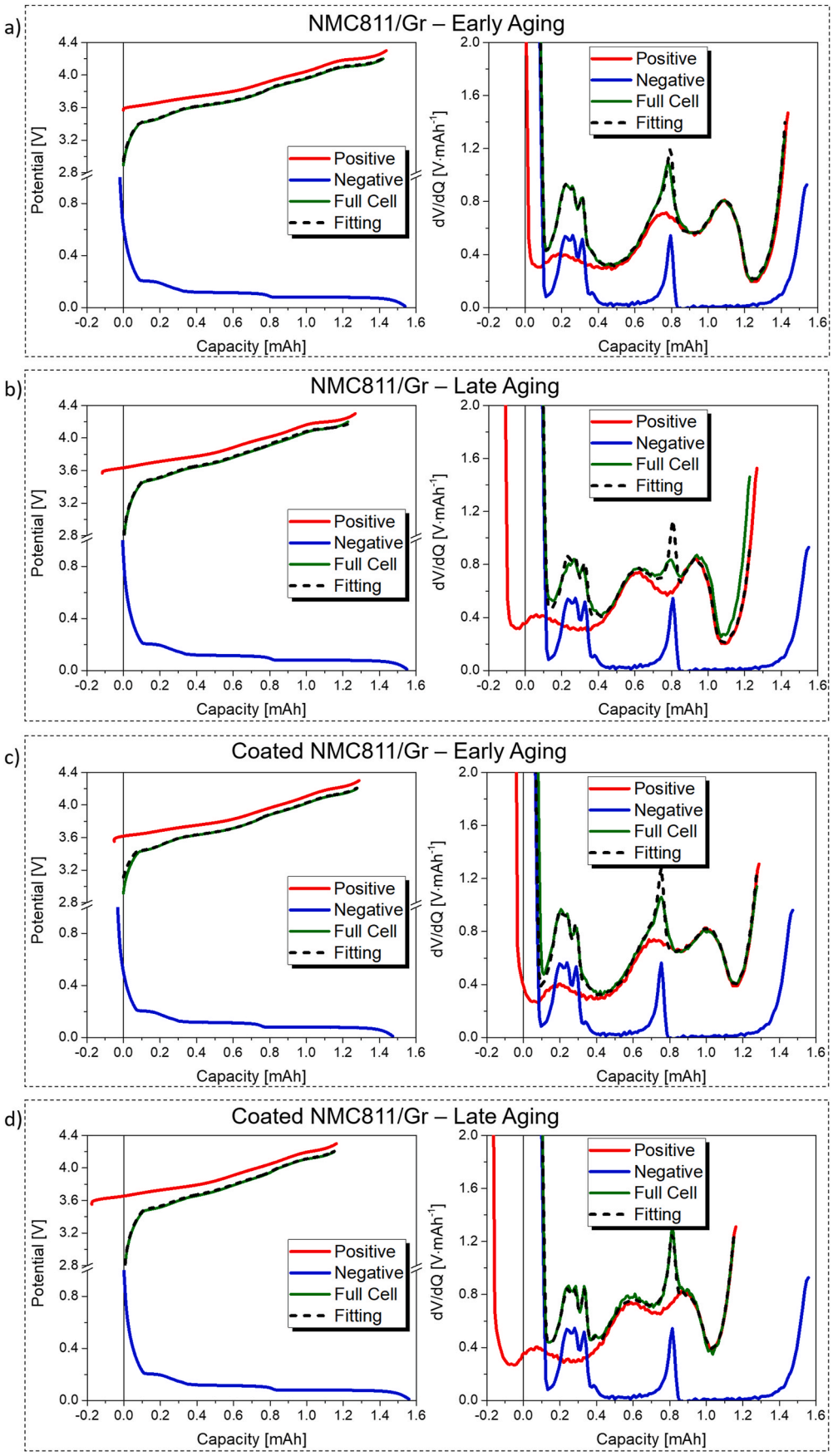


Fig. 2. V vs Q and dV/dQ vs Q fittings of a) NMC811/Gr cell first control step, b) NMC811/Gr cell last control step, c) Coated NMC811/Gr cell first control step, and d) Coated NMC811/Gr cell last control step.

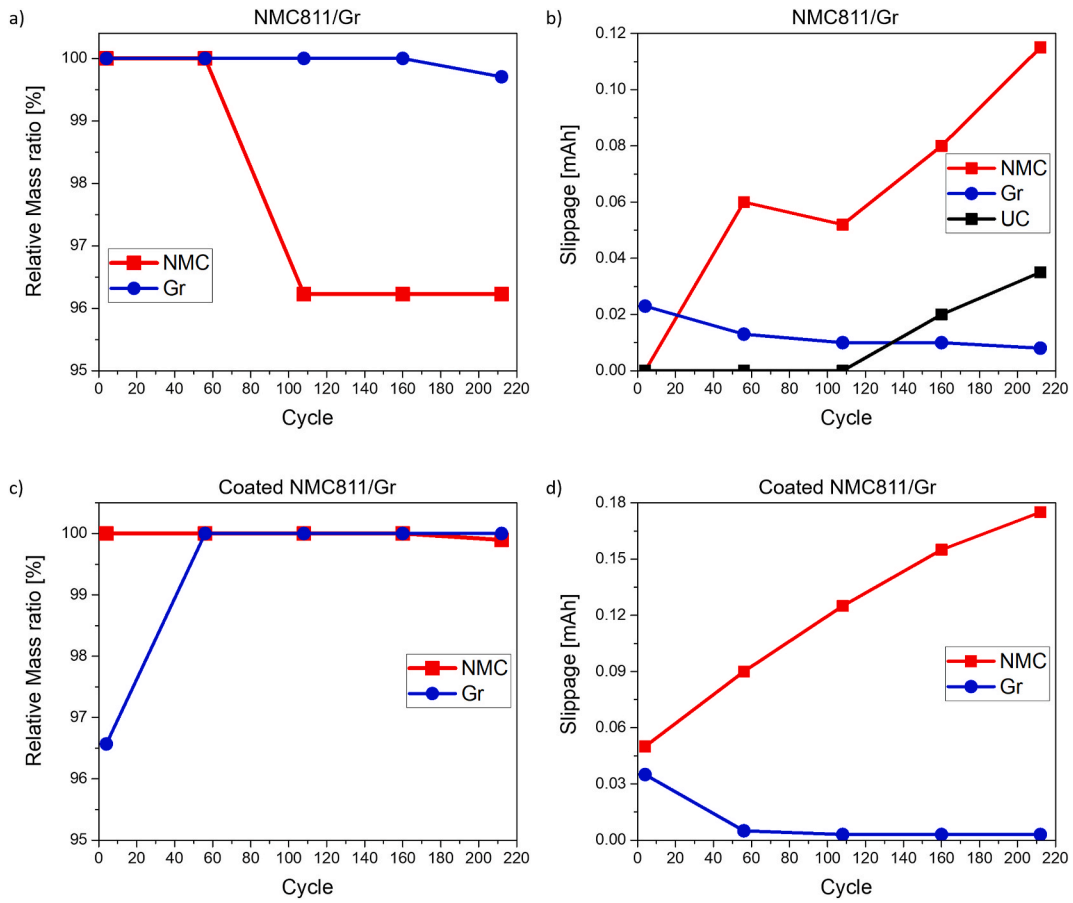


Fig. 3. Data obtained during control steps analysis. a) NMC811/Gr cell electrodes masses, b) NMC811/Gr cell electrodes slippages, and cell undercharge, c) Coated NMC811/Gr cell electrodes masses, and d) Coated NMC811/Gr cell electrodes slippages.

presents a lower capacity exchange since potentials above 4.0 V, especially after 4.2 V, in accordance with observed capacities in cells with Gr, and possibly related to the better capacity retention, as most of the reported degradation mechanisms of Ni-rich NMC electrodes take place at higher potentials.

3.2. *Changes in the OCV V vs Q curves using differential voltage analysis*

In Fig. 2, the V vs Q and its dV/dQ vs Q fittings are presented, with the vertical line in Q = 0 marking the beginning of the full-cell charge, reference for the electrodes relative capacities. One electrode's slippage is then the amount of negative capacity relative to that mark. Comparing the OCV curves of NMC811 and Gr in the beginning and in the end of the aging, from the fittings in Fig. 2a to Fig. 2b, a clear increase of the positive electrode slippage exposes that the mechanisms of capacity fade result in LLI. For later states of aging, an OCV curve of the NMC811 electrode does not maintain its shape, specifically at potentials above 4.2 V, hindering complete fitting at high SOCs. Those changes reflect in partial suppression of capacity exchange, being referred to as NMC811 undercharge. For the Coated NMC811/Gr cell, from Fig. 2c to Fig. 2d, the LLI is equally spotted by the increase in the positive slippage and by the decrease of the initial negative slippage. The latter is present if the negative electrode is incompletely delithiated when the cell is discharged. Li^+ ions reduction in the interface electrode/electrolyte of the Gr electrode, forming a passivation layer is the major reported cause for LLI in systems containing that active material. An initially large LLI is expected for the solid electrolyte interphase (SEI) formation during the first cycles, followed by its increase upon aging [39,40]. Concerning the undercharge effect, differently from the NMC811/Gr, no undercharge was observed for this cell, which indicates that the coating prevents or minimizes mechanisms related to it.

DVA fitting qualitative measurements allow tracking not only of electrode's slippage but also of its mass variation during all the monitored control steps. Between the first and the last control steps of the NMC811/Gr and the Coated NMC811/Gr cells, the loss of capacity was 0.192 mAh out of 1.420 mAh and 0.126 mAh out of 1.277 mAh, respectively. In Fig. 3a, 3,8 % of NMC811 LAM was observed around the cycle 108, meanwhile a minimal 0,3 % LAM of Gr was detected in the last control step. Fig. 3b indicated that the magnitude of the undercharge is secondary to the LLI and it appears after NMC811 LAM is detected. It is important to add that the positive slippage is reduced in the third control step, when LAM takes place, which is an indicative that the lost NMC811 fraction was predominantly poorly lithiated, when the cell is at high SOC. LAM of Coated NMC811 in Fig. 3c is negligible, meaning that the coating impacted also the degradation mechanisms linked to that effect. The initial increase of active Gr mass was spotted in some similar cells and is hypothesized to come from incomplete electrode wetting during initial cycles, possibly at the source of their noisy charge/discharge capacity values. In Fig. 3d a smoother evolution of the slippages is related to the absence of LAM. Full access of fitting images of all control steps is available in Fig. S1 and Fig. S2 of the Supporting Information for the NMC811/Gr and Coated NMC811/Gr cells respectively.

3.3. *Monitoring kinetics degradation by coupling DVA fitting and DRT*

In Fig. 4, PEIS Nyquist plots of the cells are presented as a function of the SOC. Half-cell configurations have their SOC associated with the absolute value of capacity in the control step pulsed charge, meanwhile the full-cells have their SOC associated with each electrode's relative

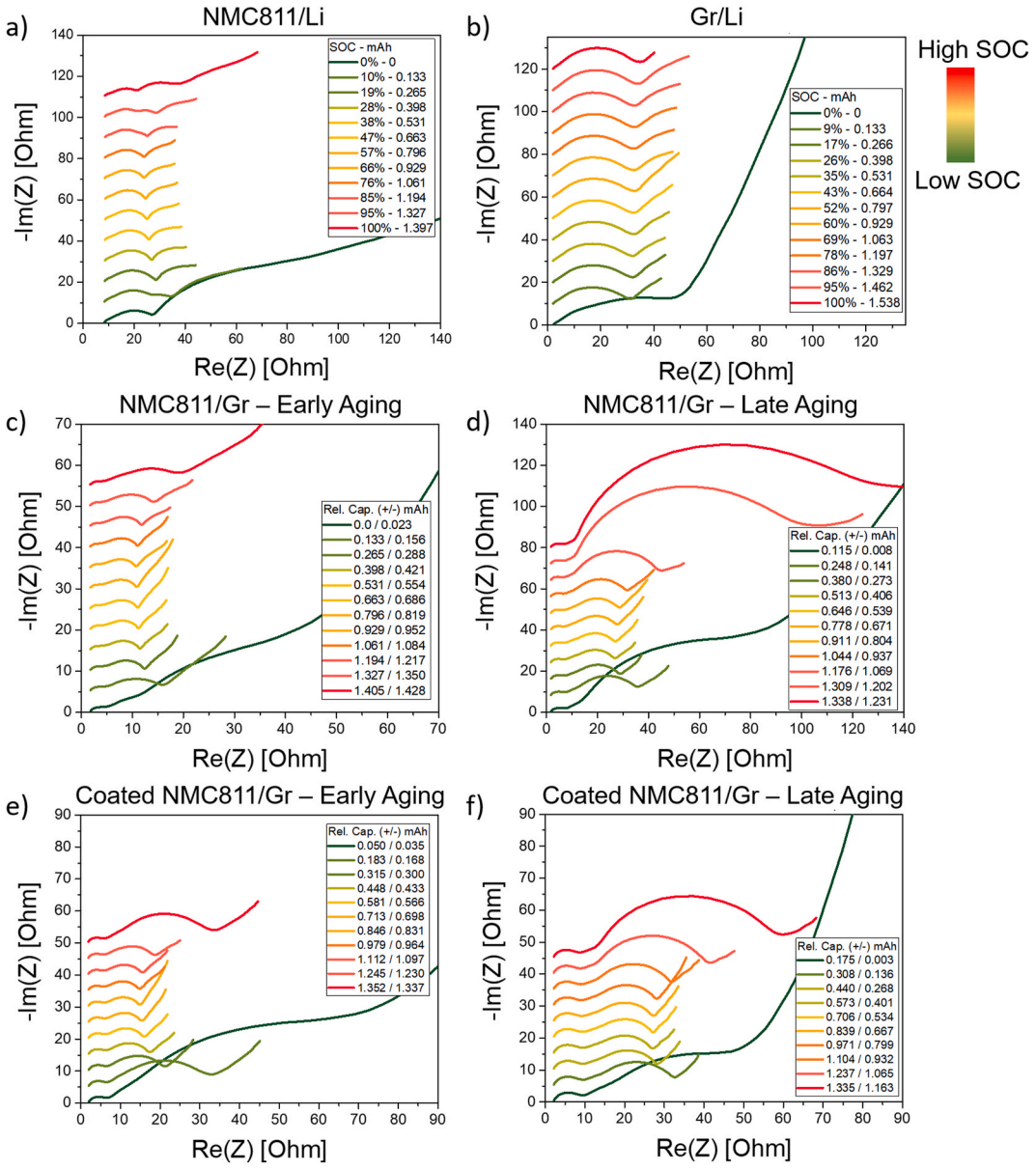


Fig. 4. Nyquist plots as function of SOC in a) NMC811/Li cell, and in b) Gr/Li cell. Nyquist plots as function of the electrodes relative capacities obtained through the V vs Q fitting for c) NMC811/Gr cell first control, d) NMC811/Gr cell last control, e) Coated NMC811/Gr cell first control, and f) Coated NMC811/Gr cell last control. Color bar indicates cell SOC and Nyquist plots of different SOC are displaced along the y-axis from each other by 5 Ω, with exception of d), that is displaced by 8 Ω.

capacity, which was obtained through the DVA fitting. Fig. 4a signs a constant diameter semi circumference at higher frequencies and at lower frequencies at least one impedance process sensitive to SOC variation, whose magnitude increases mainly during discharged state, but also when charged. Nyquist plots of Coated NMC811/Li cell present similar traits to the NMC811/Li cell with greater magnitudes for the SOC sensitive processes, and it can be accessed in Fig. S3. Fig. 4b presents for Gr/Li a marked semi circumference at the impedance portion at higher frequencies whose diameter and shape are approximately constant for all SOCs, except for its most delithiated state, when it increases considerably in size, and absence of ions reduces ionic conductivity. At 0 % SOC, it also has its lower frequencies portion modified, with a clearer linear diffusion branch. Impedance evolution of NMC811/Gr when comparing before the aging in Fig. 4c and after aging in Fig. 4d evidences the impedance increase in all SOCs, with more pronounced evolution at the end of the charge. Such SOC specific impedance rise could be at the source of the OCV V vs Q curve change of NMC811 electrode observed in the NMC811/Gr cell. That change, not present in Coated NMC811/Gr cells corroborates with the relatively moderate impedance rise of this cell, when analyzing Fig. 4e and f. Interestingly, for this cell, a decrease in the diameter of the lower frequencies semi circumference is spotted when the cell is discharged.

DRT is then exploited to disclose the number of main resistance processes and if they are associated with one specific electrode or another. That analysis is restricted to processes in the frequency range of interest (200 kHz–0.2 Hz) and not involving frequencies in which the linear diffusion branch resides. Fig. 5a and b relate NMC811/Li to 5 DRT peaks. **P0** (30 kHz) is found in all cells and can be associated with artefacts that are likely to take place in the frequency boundaries of the experiment [41]. **PP1** (4400 Hz) is SOC independent a reportedly related to active material/current collector contact resistance [42,43]. **PP2** (490–520 Hz) is in the same frequency order as the main DRT peak of the Li symmetric cell in Fig. S4, and slightly decreases in the course of the charge, to which the Li^+ ions migration through the Li counter electrode SEI is associated [44]. The SOC behavior is due to the plating process, that starts in SEI defects pits and tends to form dendrites, thus

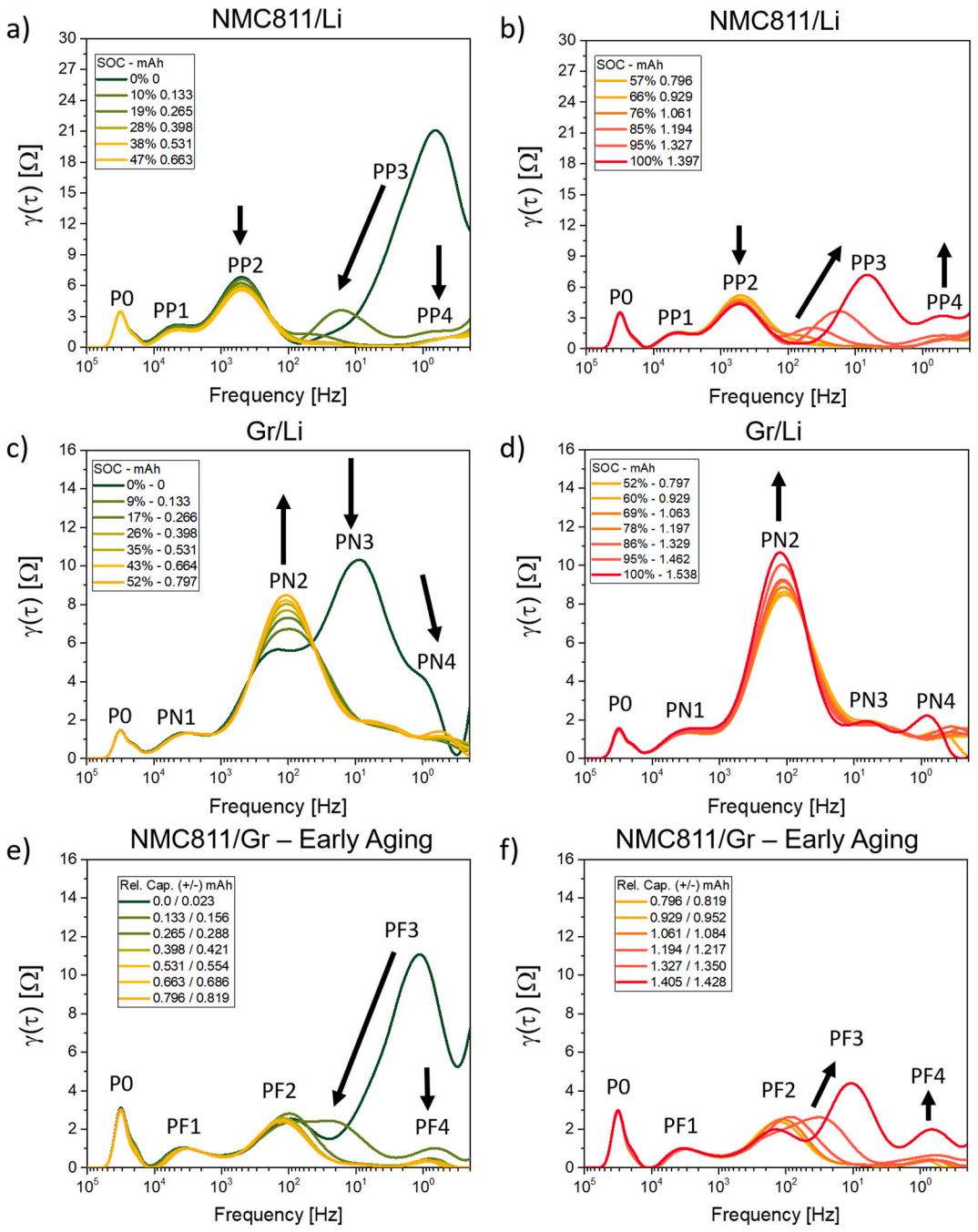


Fig. 5. DRT peaks as function of SOC. NMC811/Li cell a) low SOCs and b) high SOCs; Gr/Li cell c) low SOCs and d) high SOCs. NMC811/Gr cell as function of electrodes relative capacity during e) low SOCs and f) high SOCs. Arrows follow variations in peak height and are pointed to growing SOC.

increasing the electrode surface [45,46]. Resistance of NMC811 passivation layer, commonly independent of SOC, is possibly overshadowed by the Li passivation layer resistance if the latter is dominant for the same frequency range [31]. **PP3** (0.3 Hz–55 Hz) is the main resistance process captured by DRT technique, being almost negligible at intermediary SOC, and important for extreme SOCs, mainly when NMC811 is lithiated, pointing to NMC811 charge transfer resistance [31,42]. At lower frequencies, minor peak **PP4** (0.5 Hz) intensity follows previous peak, and its designation was secondary peak of NMC811 charge transfer resistance. In Fig. 5c and d, the Gr/Li DRT peaks have similar process associations as the NMC811/Gr cell for the same frequency ranges. **PN1** (3200 Hz) is contact resistance; **PN2** (100–165 Hz) is due to Li SEI (SOC behavior is the inverse of the seen in **PP2** as Li stripping occurs instead of plating) and might mask Gr SEI; **PN3** (3–8 Hz) is related to the Gr charge transfer, being **PN4** (0.2 Hz–1 Hz) a Gr charge transfer secondary peak [47,48].

Once all the DRT peaks from NMC811 and Gr electrodes are known as a function of their SOC, and electrodes alignment in the NMC811/Gr cell is obtained through DVA fitting, the full-cell DRT peaks can be assigned to processes of one electrode or another. From Fig. 5e comparison to Fig. 5a and c, in low SOCs, and Fig. 5f comparison to Fig. 5b and d, in high SOCs, **PF1** (3200–3800 Hz) is related to contact resistance of current collector and electrodes; **PF2** (130 Hz) is due to resistance of Gr SEI, SOC independent, confirming **PN2** had both Li and Gr SEI contributions; **PF3** (1 Hz in discharge, and 10 Hz when charged) is clearly the NMC811 charge transfer resistance due to intensity and frequency trends according to SOC, being **PF4** (0.7 Hz) a secondary peak of same process. Identical peaks matching is proceeded for the Coated NMC811/

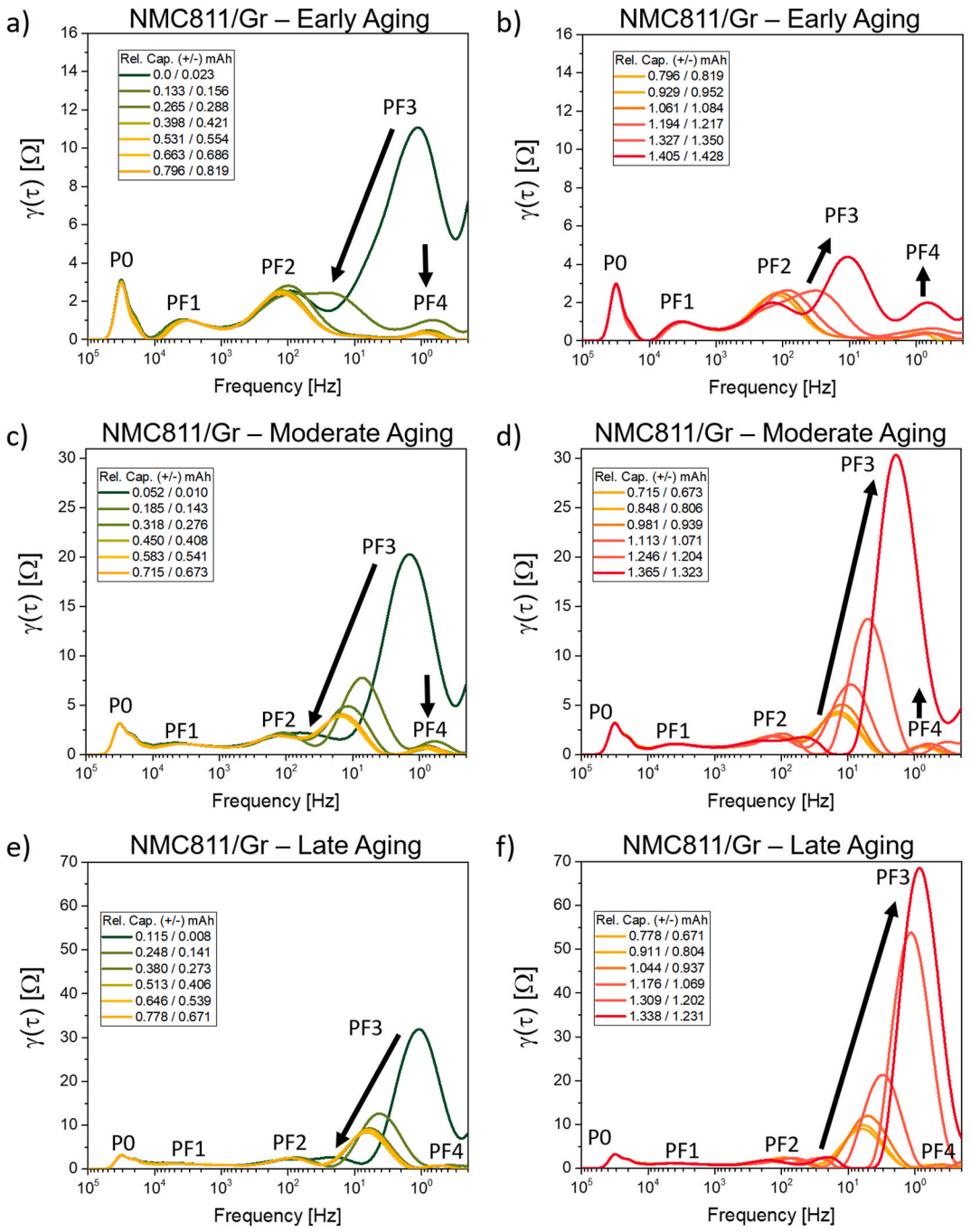


Fig. 6. DRT peaks of NMC811/Gr cell in first control step a) low SOCs and b) high SOCs, in third control step a) low SOCs and d) high SOCs, and in last control step e) low SOCs and f) high SOCs.

Gr cell, in Fig. S5, with the difference of greater charge transfer resistance of the Coated NMC811 electrode before aging. In all cases, masses of negative and positive active materials in full-cells and half-cells are similar, relative capacities in the full-cell can be approximately related to SOC capacities in half-cells DRT peaks and Nyquist plots.

Fig. 6 follows the DRT peaks of the NMC811/Gr cell before, in the middle and in the end of the aging protocol, without changes of the peak's assignments. The observed impedance rise is due to degradation mechanisms affecting the NMC811 electrode charge transfer, whose peak **PF3** assumes important magnitude even at intermediary SOCs since the middle of the aging protocol (Fig. 6c and d). Charge transfer resistance grows mainly at extreme SOCs (Fig. 6e and f), being severely impacted in the end of the charge, and possibly the source of the NMC811 OCV V vs Q curve shape change that caused the undercharge effect. Applying the same methodology to the Coated NMC811/Gr cell, in Fig. 7a and b, before the aging, same peaks **P0**, **PF1**, **PF2**, **PF3** and **PF4** observed in the NMC811/Gr are present, to which the same resistance processes are assigned (assignments in Fig. S5). Again, NMC811 charge transfer resistance holds a major role in cell total resistance for the whole aging. Nevertheless, impact of the coating is seen in minimizing this resistance growth, as followed in Fig. 7c–f. It even results in a virtual NMC811 charge transfer resistance decrease at 0 % SOC (see Fig. 7a, c and e), that occurs because LLI causes increase of positive electrode slippage and thus drives the highly resistive NMC811 lithiated states from the effective capacity window of the full-cell.

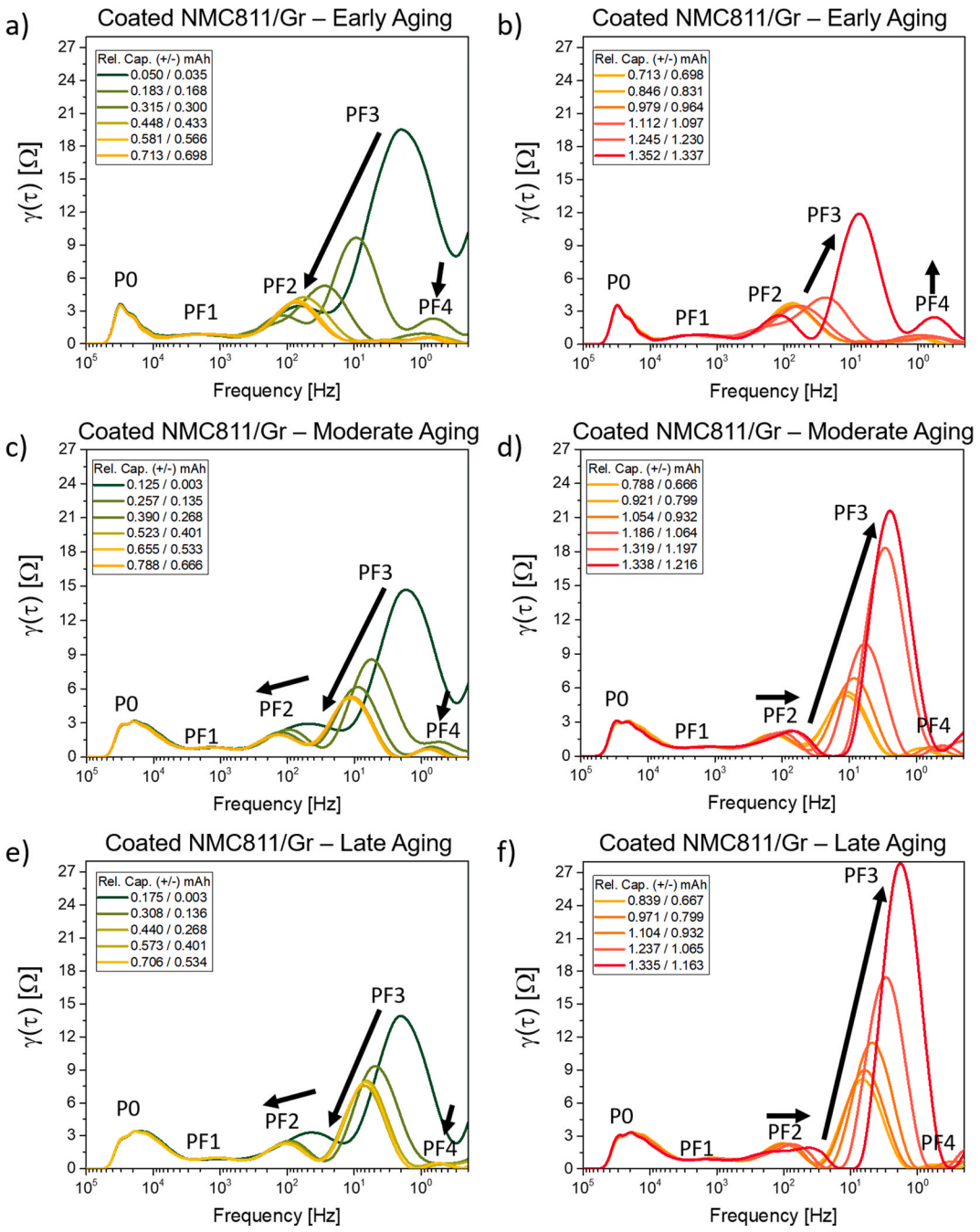


Fig. 7. DRT peaks of Coated NMC811/Gr cell in first control step a) low SOCs and b) high SOCs, in third control step a) low SOCs and d) high SOCs, and in last control step e) low SOCs and f) high SOCs.

3.4. Prospective effects of coating in degradation mechanisms

NMC811 LAM was minimized after the coating and, based on the results of DVA and DRT, it is suggested for the analyzed NMC811/Gr cells a synergy of the most reported mechanisms leading to this effect: particle cracking and inactive species formation on the electrode/electrolyte interface. Ni-rich NMCs during the delithiation experience anisotropic lattice expansion followed by a contraction around 4.2 V that eventually lead to strain in the boundaries of primary particles, and thus cracks in the secondary particles [10,49]. Cracks themselves do not cause LAM if not followed by electrical disconnection of the particles from the current collector, and their formation can reverse during the process of lithiation in the initial cycles. However, they promote electrolyte permeation in the electrode, and the reactivity in this interface. Conversion of NMC into spinel and rock-salt insulant structures results in direct LAM and in the observed charge transfer increase [49,50]. Observed undercharge seen at high SOCs is related to interfacial strain of thick rock-salt layers that hinder NMC from contraction at the end of the charge, finally changing its OCV curve, even at low current densities [51]. Addition of coating is proposed to act by turning the electrode surface less reactive to electrolyte and by hindering the capacity exchange when the positive electrode is at potentials above 4.2V, which turns the structure collapse milder and reduces electrolyte permeation. The capacity penalty of the coating is compensated by the deacceleration of electrode inactivation and impedance rise, quantified in (Fig. 8). Resistance processes of both cells in early, moderate and late aging states of the cycling were obtained by the areas of each DRT peak between two local minima.

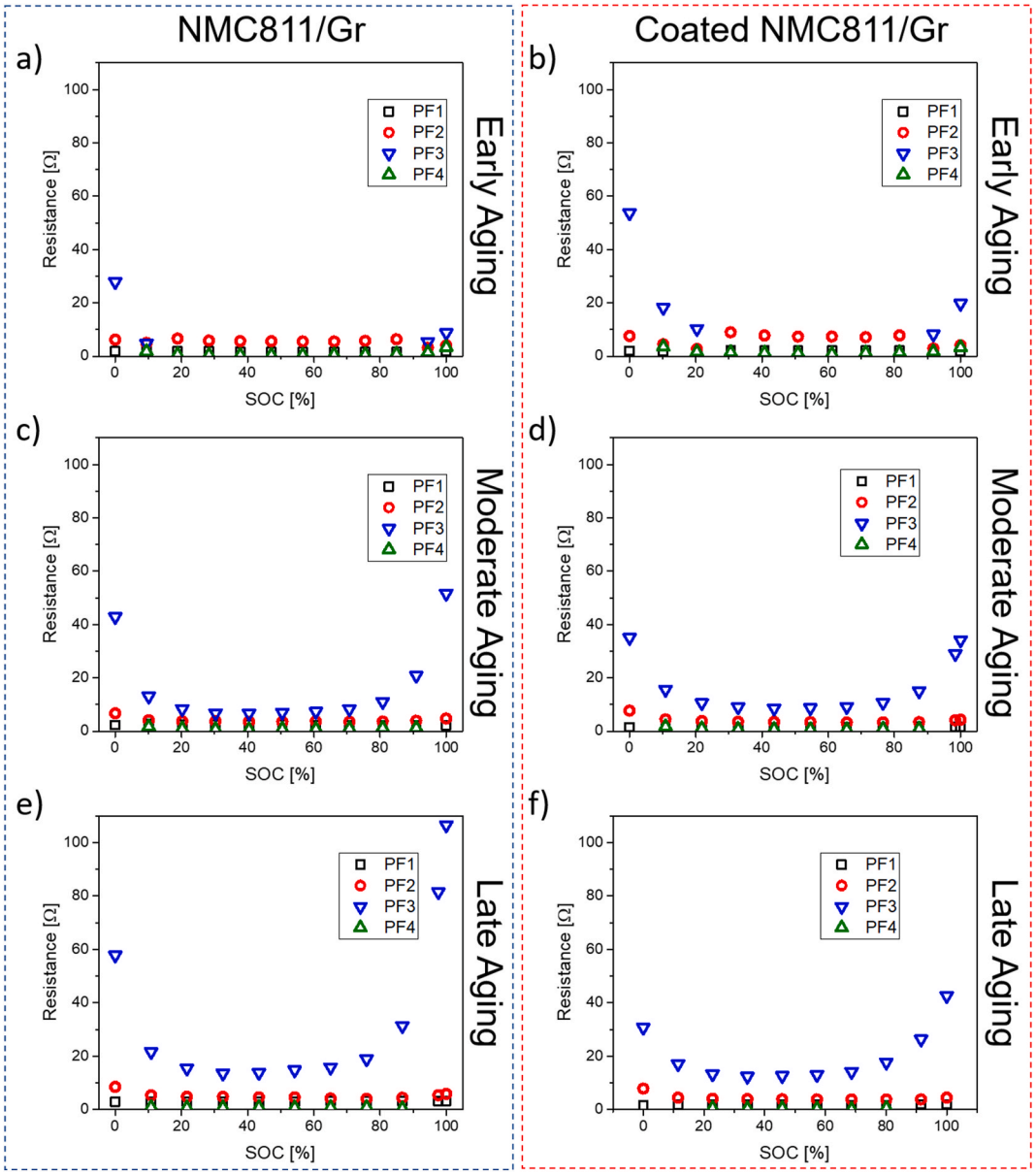


Fig. 8. DRT peak area (resistance) of processes labeled PF1, PF2, PF3 and PF4 during the first control step of a) NMC811/Gr cell and of b) Coated NMC811/Gr cell; during the third control step of c) NMC811/Gr cell and of d) Coated NMC811/Gr cell; during last control step of e) NMC811/Gr cell and of f) Coated NMC811/Gr cell.

4. Conclusion

The impact of coating the positive electrode was analyzed by comparing a NMC811/Gr and a coated NMC811/Gr cell, using electrochemical techniques. The application of an aging protocol coupling DVA fitting and DRT techniques was shown to be a non-invasive method to track degradation effects during cell operation, in terms of the thermodynamics and the kinetics from each electrode. The coating limited the NMC811 electrode delithiation to potentials above 4.2V, but this reduced capacity, as proposed in this work, smoothed volume variation and thus particle cracking and electrolyte permeation. Therefore, it minimized active material conversion to spinel and rock-salt formation, sources of LAM, undercharge at high SOC and positive electrode charge transfer resistance increase, which increased the capacity and power retention of the cell during cycling. The suggested processes were based on literature-reported degradation mechanisms for the studied materials, whose effects were closely aligned with the observed NMC811 loss of mass and charge transfer increase, more pronounced at high SOC. Although only other techniques such as XRD, XPS, SEM and others can confirm, DVA coupled with DRT succeeds in providing robust insights into LLI, LAM and impedance rise in each electrode. One of the detailed pieces of information obtained from the used approach was relating the decrease in the resistance of the coated NMC811/Gr cell in low SOCs at aging advances to the positive electrode slippage. This virtual power capability improvement in the discharged cell came from the growing absence of the NMC811 with high levels of lithiation, highly resistive, from the effective capacity window of the cell as LLI increases, highlighting the importance of studies covering different SOCs and precising electrodes slippages. The presented electrochemistry methodology found useful application in evaluating the impact of a NMC811 coating on the capacity and resistance of a cell during different stages of its life cycle, non-invasively and in operando conditions. All those characteristics turn coupling DVA fitting to the DRT a resourceful approach in the process of optimizing electrodes coatings and can be equally employed to compare cell general degradation under different parameters such as electrolyte, binders, electrode composition and cycling conditions. In

the next steps of this work, that approach is studied in cells with blended electrodes, that bring more complexity to the analysis of the presented techniques.

CRediT authorship contribution statement

Matheus Leal de Souza: Writing – review & editing, Writing – original draft, Methodology, Investigation, Formal analysis, Data curation, Conceptualization. **Mathieu Morcrette:** Writing – review & editing, Validation, Supervision, Project administration, Methodology, Investigation, Funding acquisition, Formal analysis.

Declaration of competing interest

The authors declare the following financial interests/personal relationships which may be considered as potential competing interests: Matheus Leal de Souza reports financial support was provided by Horizon 2020 European Innovation Council Fast Track to Innovation. Matheus Leal de Souza reports a relationship with Horizon 2020 European Innovation Council Fast Track to Innovation that includes: funding grants. Author was funded by the BIG-MAP project, which has received funding from the European Union's Horizon 2020 research and innovation program under grant agreement No. 957189 If there are other authors, they declare that they have no known competing financial interests or personal relationships that could have appeared to influence the work reported in this paper.

Acknowledgements

This project has received funding from the European Union's Horizon 2020 research and innovation program under grant agreement No.957189. The authors thank Prof. Patrice Simon (Université Paul Sabatier Toulouse III – France) and Dr. Alexis Grimaud (Boston College United States) for the insightful discussions taken along the project. The authors acknowledge the funding from ANR through the STORE-EX Labex project ANR-10-LABX-76-01.

Appendix A. Supplementary data

Supplementary data to this article can be found online at https://doi.org/10.1016/j.jpowsour.2025.237184.

Data availability

Data will be made available on request.

References

[1] J.-M. Tarascon, M. Armand, Nature 414 (2001) 359–367.
[2] D. Larcher, J.-M. Tarascon, Nat. Chem. 7 (2015) 19–29.
[3] J. Zhao, A.F. Burke, Batteries 8 (2022) 142.
[4] J.B. Goodenough, K.-S. Park, J. Am. Chem. Soc. 135 (2013) 1167–1176.
[5] T. Placke, R. Kloepsch, S. Dühnen, M. Winter, J. Solid State Electrochem. 21 (2017) 1939–1964.
[6] J. Kim, H. Lee, H. Cha, M. Yoon, M. Park, J. Cho, Adv. Energy Mater. 8 (2018) 1702028.
[7] H.-J. Noh, S. Youn, C.S. Yoon, Y.-K. Sun, J. Power Sources 233 (2013) 121–130.
[8] R. Jung, M. Metzger, F. Maglia, C. Stinner, H.A. Gasteiger, J. Phys. Chem. Lett. 8 (2017) 4820–4825.
[9] R. Pan, E. Jo, Z. Cui, A. Manthiram, Adv. Funct. Mater. 33 (2023) 2211461.
[10] C.S. Yoon, H.-H. Ryu, G.-T. Park, J.-H. Kim, K.-H. Kim, Y.-K. Sun, J. Mater. Chem. A 6 (2018) 4126–4132.
[11] B. Han, B. Key, S.H. Lapidus, J.C. Garcia, H. Iddir, J.T. Vaughey, F. Dogan, ACS Appl. Mater. Interfaces 9 (2017) 41291–41302.
[12] T. Li, X.-Z. Yuan, L. Zhang, D. Song, K. Shi, C. Bock, Electrochem. Energy Rev. 3 (2020) 43–80.
[13] C.S. Yoon, U.-H. Kim, G.-T. Park, S.J. Kim, K.-H. Kim, J. Kim, Y.-K. Sun, ACS Energy Lett. 3 (2018) 1634–1639.
[14] C. Liu, Z. Neale, G. Cao, Mater. Today 19 (2016) 109–123.
[15] M. Dubarry, V. Svoboda, R. Hwu, B.Y. Liaw, Electrochem. Solid State Lett. 9 (2006) A454.
[16] I. Bloom, A.N. Jansen, D.P. Abraham, J. Knuth, S.A. Jones, V.S. Battaglia, G. L. Henriksen, J. Power Sources 139 (2005) 295–303.
[17] C.R. Birkl, M.R. Roberts, E. McTurk, P.G. Bruce, D.A. Howey, J. Power Sources 341 (2017) 373–386.
[18] P. Arora, R.E. White, M. Doyle, J. Electrochem. Soc. 145 (1998) 3647.
[19] W.M. Dose, C. Xu, C.P. Grey, M.F.L. De Volder, Cell Reports Physical Science 1 (2020) 100253.
[20] H. Dahn, A. Smith, J. Burns, D. Stevens, J. Dahn, J. Electrochem. Soc. 159 (2012) A1405–A1409.
[21] I. Bloom, L.K. Walker, J.K. Basco, D.P. Abraham, J.P. Christophersen, C.D. Ho, J. Power Sources 195 (2010) 877–882.
[22] A.J. Smith, H.M. Dahn, J.C. Burns, J.R. Dahn, J. Electrochem. Soc. 159 (2012) A705.
[23] T. Waldmann, B.-I. Hogg, M. Wohlfahrt-Mehrens, J. Power Sources 384 (2018) 107–124.
[24] C. Heubner, T. Liebmann, C. Lämmel, M. Schneider, A. Michaelis, Batteries & Supercaps 5 (2022) e202100171.
[25] E. Ivers-Tiffée, A. Weber, J. Ceram. Soc. Jpn. 125 (2017) 193–201.
[26] M.A. Danzer, Batteries 5 (2019) 53.
[27] J. Illig, M. Ender, T. Chrobak, J.P. Schmidt, D. Klotz, E. Ivers-Tiffée, J. Electrochem. Soc. 159 (2012) A952.
[28] T.H. Wan, M. Saccoccio, C. Chen, F. Ciucci, Electrochim. Acta 184 (2015) 483–499.
[29] H. Schichlein, A.C. Müller, M. Voigts, A. Krügel, E. Ivers-Tiffée, J. Appl. Electrochem. 32 (2002) 875–882.
[30] K. Pan, F. Zou, M. Canova, Y. Zhu, J.-H. Kim, J. Power Sources 479 (2020) 229083.
[31] P. Shafiei Sabet, D.U. Sauer, J. Power Sources 425 (2019) 121–129.
[32] P. Shafiei Sabet, G. Stahl, D.U. Sauer, J. Power Sources 472 (2020) 228189.
[33] M.L. de Souza, M. Duquesnoy, M. Morcrette, A.A. Franco, Batteries & Supercaps 6 (2023) e202200378.
[34] J. Vetter, P. Novák, M.R. Wagner, C. Veit, K.-C. Möller, J.O. Besenhard, M. Winter, M. Wohlfahrt-Mehrens, C. Vogler, A. Hammouche, J. Power Sources 147 (2005) 269–281.
[35] H. Kato, Y. Kobayashi, H. Miyashiro, J. Power Sources 398 (2018) 49–54.
[36] T. Dagger, J. Kasnatscheew, B. Vortmann-Westhoven, T. Schwieters, S. Nowak, M. Winter, F.M. Schappacher, J. Power Sources 396 (2018) 519–526.
[37] T. Hüfner, M. Oldenburger, B. Bedürftig, A. Gruhle, J. Energy Storage 24 (2019) 100790.
[38] B.A. Boukamp, JPhys Energy 2 (2020) 042001.
[39] S.J. An, J. Li, C. Daniel, D. Mohanty, S. Nagpure, D.L. Wood, Carbon 105 (2016) 52–76.
[40] D. Aurbach, M.D. Levi, E. Levi, A. Schechter, J. Phys. Chem. B 101 (1997) 2195–2206.
[41] M. Hahn, S. Schindler, L.-C. Triebs, M.A. Danzer, Batteries 5 (2019) 43.
[42] Y. Zhao, V. Kumtepeli, S. Ludwig, A. Jossen, J. Power Sources 530 (2022), https://doi.org/10.1016/j.jpowsour.2022.231250.
[43] X. Zhou, J. Huang, Z. Pan, M. Ouyang, J. Power Sources 426 (2019) 216–222.
[44] S. Drvarič Talian, J. Bobnar, A.R. Sinigoj, I. Humar, M. Gaberšček, J. Phys. Chem. C 123 (2019) 27997–28007.
[45] K.-H. Chen, K.N. Wood, E. Kazyak, W.S. LePage, A.L. Davis, A.J. Sanchez, N. P. Dasgupta, J. Mater. Chem. A 5 (2017) 11671–11681.
[46] C. Rabette, Determination of the Transport Properties of Liquid Electrolytes for Lithium-Ion Batteries Using a Multi-Electrode Electrochemical Cell, 2022.
[47] M. Steinhauer, S. Risse, N. Wagner, K.A. Friedrich, Electrochim. Acta 228 (2017) 652–658.
[48] P. Iurilli, C. Brivio, V. Wood, Energy Technol. 10 (2022), https://doi.org/10.1002/ente.202200547.
[49] C. Busà, M. Belekoukia, M.J. Loveridge, Electrochim. Acta 366 (2021) 137358.
[50] S. Lee, L. Su, A. Mesnier, Z. Cui, A. Manthiram, Joule 7 (2023), https://doi.org/10.1016/j.joule.2023.09.006.
[51] C. Xu, K. Märker, J. Lee, A. Mahadevegowda, P.J. Reeves, S.J. Day, M.F. Groh, S. P. Emge, C. Ducati, B. Layla Mehdi, C.C. Tang, C.P. Grey, Nat. Mater. 20 (2021) 84–92.